Systems & Control Transactions

Research Article
Foundations of Computer Aided Process Design (FOCAPD 2024)
Breckenridge, Colorado, USA. July 14-18, 2024
Peer Reviewed Conference Proceeding

PSE PRESS

Modeling the Maximization of Waste Heat Use in a Liquid Solvent Direct Air Capture Plant Through Hydrogen Production

Erick O. Arwa[a*] and Kristen R. Schell[a]

[a] Carleton University, Department of Mechanical and Aerospace Engineering, Ottawa, Ontario, Canada
* Corresponding Author: erickarwa@cmail.carleton.ca.

ABSTRACT

Direct air capture (DAC) of carbon dioxide is a promising technology to enable climate change mitigation. The liquid solvent DAC (LSDAC) process is one of the leading technologies being piloted. However, LSDAC uses a high-temperature regeneration process which requires a lot of thermal energy. Although current LSDAC designs incorporate pre-heat cyclones and a heat recovery steam generator to enable heat recovery, these do not maximize the use of the heat in the products of calcination. In this paper, a linear optimization model is developed to minimize energy cost in a LSDAC that is powered by renewable energy and natural gas. First, the material flow network is modified to include a heat exchanger (HX) and water supply to a proton exchange membrane (PEM) electrolyser. Mass and energy balance constraints are then developed to include the water flow as well as the energy balance at the PEM and the HX. Results show that about 911 tonnes of hydrogen could be produced over 336 hours of operation using a 136MW PEM. Further analysis reveals that hydrogen production is only prioritized if the value is higher than the cost of natural gas.

Keywords: Climate change, Direct air capture, Hydrogen, Negative emission technologies, PEM

INTRODUCTION

To forestall a possible climate crisis, negative emission technologies (NETs) such as direct air capture (DAC) of $CO_{2(g)}$ from the atmosphere are considered a necessary addition to other mitigation measures [1]. This is due to its ability to capture the already emitted carbon from the atmosphere independent of the origin of the emission. Also, DAC is likely to reduce the cost of achieving net-zero power grids [2], [3]. DAC has special advantages over other NETs such as traceability, controllability, and modularity. Two crucial DAC technologies are currently being piloted in various parts of the globe: liquid solvent DAC (LSDAC) and solid sorbent DAC. Compared to the solid sorbent technologies, the LSDAC has a slightly lower energy requirement per tonne of $CO_{2(g)}$, better scalability and continuity of operation [1]. Further, LSDAC uses mature chemical process technologies such as calcium looping (CL) [4].

Despite the promising features of LSDAC, it faces several challenges. First, its capture rate is heavily influenced by climate as the liquid solvent may freeze at temperatures below 0 °C [5]. Second, the high-temperature regeneration process is energy intensive requiring a stable power supply necessitating the use of high capacity factor power generation technologies, most of which depend on fossil fuels. DAC energetics is an important research agenda that would enable efficient integration of the technology into the energy system. Among the aspects of improving the energy profile of LSDAC is reducing the energy required for regeneration through electrochemical processes [6]. Another important aspect is making the regeneration process flexible so that it could be powered using renewable energy (RE) sources, which are intermittent by nature [7]. One technique of improving DAC energetics that is missing in the literature is the full utilization of heat recovered from the LSDAC. In [8], $H_{2(g)}$ is produced using waste heat from an organic Rankine cycle generator. The waste heat is useful in providing the thermal needs of the PEM and raising the temperature of

the inflowing water to the PEM's operating temperature, thereby improving its performance [9], [10].

Keith et al [4] discussed several heat integration techniques that enhanced the use of heat recovered from the calciner and the slaker. In their model, heat is recovered from outgoing $CO_{2_{(g)}}$ from the calciner to pre-heat the incoming $CaCO_3$ pellets from the pellet reactor to 650 °C through two cyclones. Another cyclone is used to recover heat from CaO to pre-heat oxygen from the air separation plant (ASP) to 674 °C. Heat is also recovered from these two substances and the steam slaker through a heat recovery steam generator to produce steam which is used to drive a steam turbine to produce electricity for the plant. However, this elaborate heat recovery scheme still leaves a lot of thermal energy wasted. For instance, after all the heat recovery processes, $CO_{2_{(g)}}$ is still at 325 °C, which has energy that could still power the system if properly integrated. Furthermore, if the system is all electric, there is no need for an ASP, thus freeing the heat from CaO for reuse in the process.

This paper proposes the use of the recovered heat from the products of calcination to produce $H_{2_{(g)}}$. It is an improvement of [7], where a linear programming (LP) model was proposed to lower energy costs in the LSDAC plant by flexibly scheduling regeneration process to maximize the utilization of RE in the plant. First, the process flow is modified to include a heat exchanger (HX) and water supply to a proton exchange membrane (PEM) electrolyser. Additional constraints are then developed to model the additional water flow as well as the energy balance at the PEM and the HX.

METHODOLOGY

Process Flow Design of the Proposed DAC Plant

Designed by Keith et al [4], a typical liquid solvent DAC plant has two major loops. The first loop – the potassium cycle – starts at the air contactor where $KOH_{(aq)}$ reacts with $CO_{2_{(g)}}$ from the air, producing $K_2CO_{3_{(aq)}}$, which is reacted with $Ca(OH)_{2_{(aq)}}$ in the pellet reactor, thereby regenerating the $KOH_{(aq)}$ to complete the cycle. The second cycle starts with the thermal decomposition of $CaCO_{3_{(s)}}$ from the pellet reactor in a calciner to regenerate the captured $CO_{2_{(g)}}$. This is followed by slaking of the resultant CaO_s using steam to produce $Ca(OH)_{2_{(aq)}}$ for use in the pellet reactor, thus completing the second cycle. In [7], the second loop is remodeled to include solids storage silos to enable flexible scheduling of the calcination process to maximize RE utilization in the energy-intensive process. In this paper, a further modification is proposed to improve the utilization of the energy contained in the $CO_{2_{(g)}}$ and CaO_s from the calciner. This is done by including $H_{2_{(g)}}$ production in the process flow to make use of the waste heat. Pre-heat cyclones included by Keith et al [4] are utilized here except for the one that is associated with the air separation plant, which is not necessary in our electrified calciner. The process flow of the proposed DAC plant with an integrated PEM is shown in Figure 1.

Optimization Model of the Flexible DAC with Hydrogen Production

A new model is developed to include $H_{2_{(g)}}$ production constraints. The model is defined as follows:

$$min\ F\ = \sum_{t\in T}\left(C_{ng}p_t^{ng}\Delta t + C_iC_cp_t^{ng}\Delta t - C_{H_2}m_t^{H_2}\right) \quad (1)$$

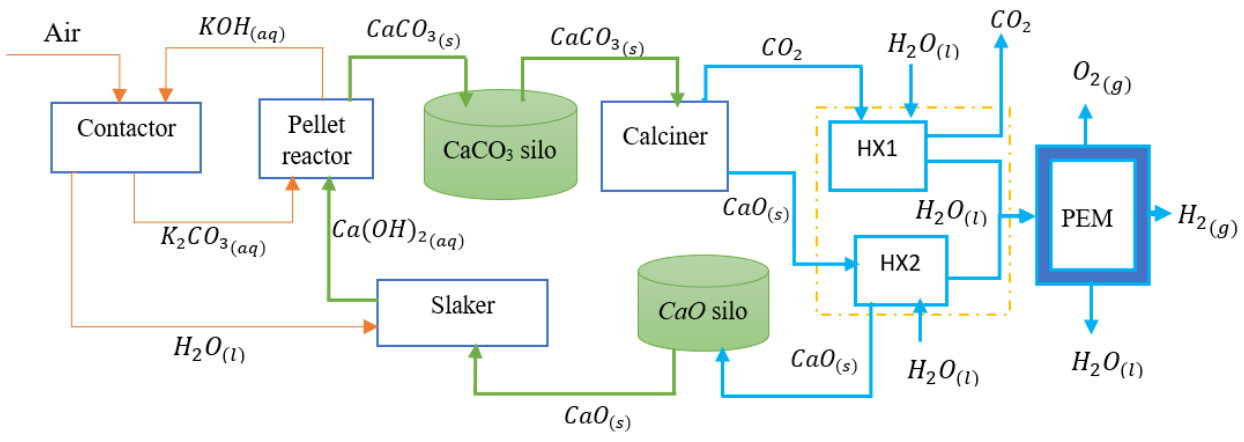

Figure 1: The process flow of the proposed DAC plant with an integrated PEM.

$$p_t^{pem} \geq \alpha m_t^{H_2O,pem}, \quad \forall t \in T \tag{2}$$

$$m_t^{H_2O,out} = m_t^{H_2O,in} - m_t^{H_2O,pem}, \quad \forall t \in T \tag{3}$$

$$m_t^{H_2} = \frac{2}{18} m_t^{H_2O,pem}, \quad \forall t \in T \tag{4}$$

$$m_t^{O_2} = \frac{16}{18}\left(m_t^{H_2O,pem}\right), \quad \forall t \in T \tag{5}$$

$$p_t^{pem} + m_t^{H_2O,in} c^{H_2O}\left(T_{hx}^{H_2O} - T_a\right) = \beta m_t^{H_2O,pem} + m_t^{H_2} c^{H_2}\left(T_{pem} - T_a\right) + m_t^{O_2} c^{O_2}\left(T_{pem} - T_a\right) + m_t^{H_2O,out} c^{H_2O}\left(T_{pem} - T_a\right), \quad \forall t \in T \tag{6}$$

$$m_t^{H_2O,in} c^{H_2O}\left(T_{hx}^{H_2O} - T_a\right) = \eta x_t^c \left(0.44 c^{O_2}\left(T_{dac}^{CO_2} - T_{hx}^{CO_2}\right) + 0.56 c^{CaO}\left(T_{dac}^{CaO} - T_{hx}^{CaO}\right)\right), \quad \forall t \in T \tag{7}$$

$$P^{df} + p_t^{dv} + p_t^{pem} = p_t^{ng} + p_t^{w} + p_t^{s}, \quad \forall t \in T \tag{8}$$

$$p_t^{dv} = \phi m_t^{CO_2}, \quad \forall t \in T \tag{9}$$

$$0 \leq p_t^{w} \leq P_{max}^{w}, \quad \forall t \in T \tag{10}$$

$$0 \leq p_t^{s} \leq P_{max}^{s}, \quad \forall t \in T \tag{11}$$

$$0 \leq p_t^{ng} \leq P_{max}^{ng}, \quad \forall t \in T \tag{12}$$

$$m_t^{cc} = m_{t-1}^{cc} + r_t^{cc}\Delta t, \quad \forall t \in T \tag{13}$$

$$-R_{max}^{cc} \leq r_t^{cc} \leq R_{max}^{cc}, \quad \forall t \in T \tag{14}$$

$$0 \leq m_t^{cc} \leq M_{max}^{cc}, \quad \forall t \in T \tag{15}$$

$$m_t^{cc} = 0, \; t \in \{0, T\} \tag{16}$$

$$m_t^{c} = m_{t-1}^{c} + r_t^{c}\Delta t, \quad \forall t \in T \tag{17}$$

$$-R_{max}^{c} \leq r_t^{c} \leq R_{max}^{c}, \quad \forall t \in T \tag{18}$$

$$0 \leq m_t^{c} \leq M_{max}^{c}, \quad \forall t \in T \tag{19}$$

$$m_0^{c} = m_T^{c} \tag{20}$$

$$x_t^{c} \leq X_{max}^{c}, \quad \forall t \in T \tag{21}$$

$$r_t^{cc} + x_t^{c} = X^{p}, \quad \forall t \in T \tag{22}$$

$$0.56 x_t^{c} = X^{s} + r_t^{c}, \quad \forall t \in T \tag{23}$$

$$m_t^{CO_2} = 0.44 x_t^{c}\Delta t, \quad \forall t \in T \tag{24}$$

The objective of the model is to minimize energy cost as given by equation (1), where the sales of hydrogen is subtracted to encourage heat recovery. Equation (2)-(7) are the PEM plant constraints defined as follows: the PEM electrical energy supply constraint (2); the water flow balance for the PEM (3); the $H_{2_{(g)}}$ output (4); $O_{2_{(g)}}$ output (5); power equilibrium at the PEM (6); and the HX thermal energy balance (7). In (2), α is the Gibb's free energy, ΔG, of water at the operating temperature (353K) in MWh/kg. This is obtained from the value of ΔG in kJ/mol expressed as [11], [12], [13]:

$$\Delta G = nF\,(1.229 - 0.0009(\tau - 298)) \tag{25}$$

where $n = 2$ is the number of electrons transferred in the electrolysis of a molecule of water, $F = 96485C$ is Faraday's constant and τ is the temperature in Kelvin. Equations (8)-(12) and (13)-(26) are the energy supply constraints and mass flow constraints for the flexible DAC plant; the reader is referred to [7] for a detailed description of these constraints. The energy supply constraints are briefly defined as follows: power equilibrium at the supply bus (8), variable calciner and compressor demand (9), wind power generator boundary (10), solar generation constraint (11), and NGG capacity constraint (12). The mass flow constraints for the DAC plant are defined as follows: $CaCO_3$ storage silo mass flow dynamics (13), silo flowrate (14) and capacity limits (15); capture rate enforcement constraint for the $CaCO_3$ silo (16), which ensures all the captured $CO_{2_{(g)}}$ is regenerated; CaO silo mass flow dynamics (17), flowrate (18) and capacity limits (19); capture rate enforcement constraint for the CaO silo (20); calciner throughput limit (21); coupling constraint between the calciner and the $CaCO_3$ silo (22); coupling constraint between the calciner and the CaO silo (23) and a constraint to compute the mass of $CO_{2_{(g)}}$ regenerated. Table 2 shows the model decision variables that are optimized.

Data

The parameters of the model are shown in Table 1. Details of the RE profiles and the DAC parameters have been provided in [7].

RESULTS AND DISCUSSION

This paper models $H_{2_{(g)}}$ production from waste heat from a liquid solvent DAC plant using a PEM. The PEM is assumed to be able to make use of all the heat recovered to produce the $H_{2_{(g)}}$, thus, the PEM size is not limiting. In this section, PEM output and the impact of this modification on the overall energy cost of the plant are discussed.

PEM Performance and Energy Consumption

Over the 336 hours modeled, which represent variation in renewable energy supply, a total of about 910,890 kg of $H_{2_{(g)}}$ is produced, which translates to about 2,711 kg/h. This level of production would need a 136 MW PEM, if losses are ignored. Given that the higher heating value (HHV) of $H_{2_{(g)}}$ is about 0.0394 MWh/kg, the output energy is close to 35,889 MWh of energy produced at an average rate of 106 MW, which is equivalent to 78.4% efficiency. This efficiency value would be lower if all the losses are considered. However, it would still result in a better efficiency compared to using the recovered heat to generate power using an organic Ranking cycle, whose efficiency is less than 30%.

Table 1: Model Parameters

Parameter	Description	Value and Units
C_c	Carbon tax	37.1 \$/tonne-CO_2
C_i	NGG carbon intensity	0.3894 tonne-CO_2/MWh
C_{H_2}	Price of $H_{2_{(g)}}$	\$/kg
C_{ng}	Cost of natural gas	27.77 \$/MWh
c^{CO_2}	Specific heat capacity of CO_2	1.065 kJ/kg/K
c^{O_2}	Specific heat capacity of O_2	0.924 kJ/kg/K
c^{H_2O}	Specific heat capacity of H_2O	4.184 kJ/kg/K
c^{H_2}	Specific heat capacity of H_2	14.493 kJ/kg/K
c^{CaO}	Specific heat capacity of CaO	0.945 kJ/kg/K
M^c_{max}	CaO silo capacity	370 tonnes
M^{cc}_{max}	$CaCO_3$ silo capacity	660 tonnes
P^{df}	Fixed DAC demand	20 MW
P^{ng}_{max}	NGG capacity	165 MW
P^{s}_{max}	Maximum PV power	110 MW
P^{w}_{max}	Maximum wind power	140 MW
R^c_{max}	CaO silo maximum flowrate	134 tonnes/h
R^{cc}_{max}	$CaCO_3$ silo maximum flowrate	240 tonnes/h
T	Optimization horizon	336h
T_a	Ambient temperature	25 ºC
$T^{CO_2}_{dac}$	Temperature of CO_2 leaving the pre-heat cyclones of DAC.	450 ºC
T^{CaO}_{dac}	Temperature of CaO leaving the calciner	900 ºC
T^{CaO}_{hx}	Temperature of CaO leaving the HX	300 ºC
$T^{H_2O}_{hx}$	Temperature of H_2O leaving the HX	80 ºC
T_{pem}	PEM operating temperature	80 ºC
X^c_{min}	Minimum calciner flowrate	20 tonnes/h
X^c_{min}	Minimum calciner flowrate	500 tonnes/h
X^p	Pellet reactor flowrate	260 tonnes/h
X^s	Slaker flowrate	145.6 tonnes/h
α	Gibb's free energy of H_2O at T_{pem}	0.00351 MWh/kg
β	Enthalpy of formation of H_2O	0.00441 MWh/kg
η	HX efficiency	0.8
ϕ	Calciner and compressor consumption	1.226 MWh/tonne-CO_2
Δt	Timestep size	1h

Table 2: Model Decision Variables

Variable	Description	Units
m^c_t	Mass of stored CaO at time, t	tonne
m^{cc}_t	Mass of stored $CaCO_3$ at time, t	tonne
$m^{CO_2}_t$	Mass of CO_2 regenerated at time, t	tonne
$m^{H_2}_t$	Mass of H_2 produced at time, t	kg
$m^{H_2O,in}_t$	Mass of H_2O flowing into the PEM at time, t	kg
$m^{H_2O,out}_t$	Mass of H_2O flowing out of the PEM at time, t	kg
$m^{H_2O,pem}_t$	Mass of H_2O electrolyzed by the PEM at time, t	kg
$m^{O_2}_t$	Mass of O_2 produced by the PEM at time, t	kg
p^{dv}_t	Variable demand of the DAC plant at time, t	MW
p^{ng}_t	Power generated by the NGG at time, t	MW
p^{pem}_t	Electrical power supplied to the PEM at time, t	MW
p^{s}_t	Solar power consumed at time, t	MW
p^{w}_t	Wind power consumed at time, t	MW
r^c_t	Mass flow rate of the CaO silo at time, t	tonne/h
r^{cc}_t	Mass flow rate of the $CaCO_3$ silo at time, t	tonne/h
x^c_t	Calciner flowrate at time, t	tonne/h

Sensitivity Analysis: Factors Affecting the Mass of Hydrogen Produced

The production of $H_{2_{(g)}}$ requires both thermal and electrical energy. Although the amount of thermal energy recovered from the calciner is constant – provided the $CO_{2_{(g)}}$ capture rate is enforced – the electrical input is derived from RE and the NGG. The objective function of the optimization model penalizes the use of NGG while encouraging the production of $H_{2_{(g)}}$. Therefore, two main factors affect the amount of $H_{2_{(g)}}$ produced.

First, if the cost of NGG is constant, the price of $H_{2_{(g)}}$ determines whether $H_{2_{(g)}}$ is produced. Observing the amount of $H_{2_{(g)}}$ produced per hour for the value of C_{H_2} ranging from 0.0 to 3.0 \$/kg, it was established that the $H_{2_{(g)}}$ production becomes attractive at $C_{H_2} =$ 1.67 \$/kg. Considering that the higher heating value (HHV) of $H_{2_{(g)}}$ is about 0.0394 MWh/kg, this price coincides with an energy price of about 42.38 \$/MWh, which is very close to but slightly above the cost of NGG power from the NGG, which is 42.22 \$/MWh. Figure 2 shows the impact of the price of $H_{2_{(g)}}$ on its hourly production rate.

The second important factor affecting the $H_{2_{(g)}}$ production rate is the NGG capacity. If the price is set at 1.67 \$/kg, increasing the NGG capacity increases the rate of $H_{2_{(g)}}$ production provided the PEM capacity is not limited. This is because the increase in NGG capacity increases the amount of energy available for $H_{2_{(g)}}$ production. The production also increases because the price of

$H_{2_{(g)}}$ is set slightly higher than the cost of energy from the NGG. Figure 3 shows the impact of the NGG capacity on $H_{2_{(g)}}$ production rate.

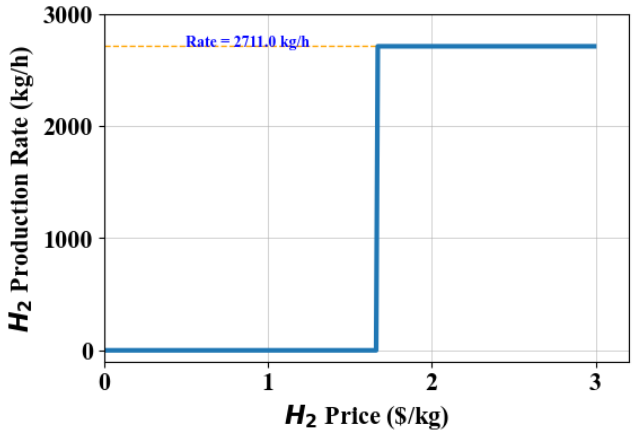

Figure 2. Impact of $H_{2_{(g)}}$ price on the production rate.

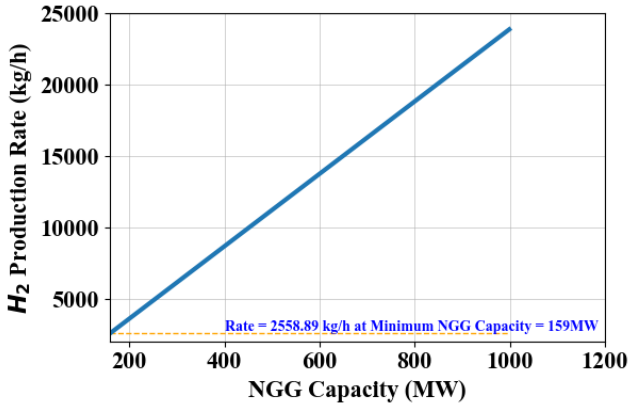

Figure 3. Impact of NGG capacity on $H_{2_{(g)}}$ production rate.

Though the rate of production of $H_{2_{(g)}}$ increases with NGG capacity, it also leads to more emission of $CO_{2_{(g)}}$, therefore, only the capacity needed to sustain the system is allowed, which is set at 165 MW.

Implications of Including the PEM on System Energy Use Dynamics

With flexibility in the $H_{2_{(g)}}$, the role of the solids storage silos in minimizing curtailment vanishes, provided the PEM size is not a limiting factor. Therefore, the silo size no longer impacts the cost of energy, which departs from the findings in [7] where the silos played a major role in curtailment reduction. This is because the cheap RE facilitates the $H_{2_{(g)}}$ production so that none of the available renewable energy is curtailed. Furthermore, including the PEM increases the energy demand considerably such that no moments of oversupply exist.

Consequently, the calciner and the NGG operate at full capacity throughout the optimization horizon. This is because there is an incentive in the objective function for increasing hydrogen production. The calciner operates at full capacity to supply the thermal demands of the PEM while the NGG supplies the electrical energy demand.

However, the PEM's output profile coincides with that of the RE. This is because RE provides cheap electrical energy for hydrogen production, which could be used for both the PEM's thermal and electrical needs. Figure 4 shows the mass of $H_{2_{(g)}}$ produced by the PEM, which aligns with RE availability and use.

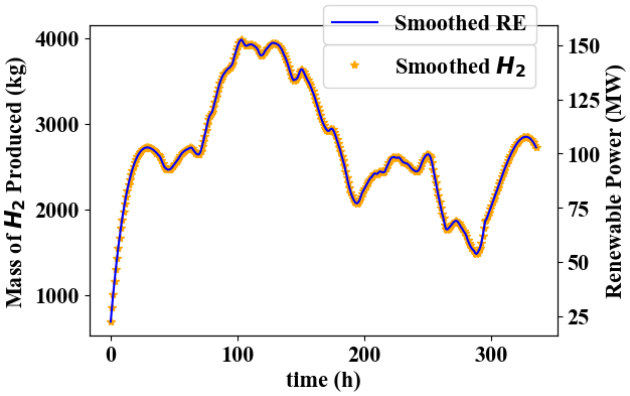

Figure 4. $H_{2_{(g)}}$ production profile alongside RE supply (Smoothing was done using Savitzky–Golay filter).

CONCLUSION

This paper presents a linear programming optimization model which was developed to incorporate a PEM in the process flow design of an LSDAC plant to maximize the use of waste heat for hydrogen production. Novel mass and energy flow constraints are developed to maintain energy and water supply to the PEM electrolyser. Results show that 911 tonnes of hydrogen could be produced over 336 hours of operation by a 136 MW PEM. Sensitivity analyses reveal that hydrogen production is only prioritized if its sale value is higher than the cost of natural gas. Under such market conditions, the production of hydrogen would only be limited by the PEM size and availability of the required electrical energy. The inclusion of the PEM also eliminates the need for solids storage silos, which were previously required to enhance process flexibility and use of variable renewable energy. Future research could develop temperature-dependent models for the PEM hydrogen output profile to enable analysis of the impact of temperature on the amount of hydrogen produced from the recovered heat.

ACKNOWLEDGEMENTS

This project was undertaken with the financial support of the Government of Canada.

REFERENCES

1. International Energy Agency, “Direct Air Capture: A key technology for net zero,” Paris, Apr. 2022. [Online]. Available: www.iea.org/t&c/
2. D. Y. Shu, S. Deutz, B. A. Winter, N. Baumgärtner, L. Leenders, and A. Bardow, “The role of carbon capture and storage to achieve net-zero energy systems: Trade-offs between economics and the environment,” Renewable and Sustainable Energy Reviews, vol. 178, May 2023, doi: 10.1016/j.rser.2023.113246.
3. J. E. T. Bistline and G. J. Blanford, “Impact of carbon dioxide removal technologies on deep decarbonization of the electric power sector,” Nat Commun, vol. 12, no. 1, Dec. 2021, doi: 10.1038/s41467-021-23554-6.
4. D. W. Keith, G. Holmes, D. St. Angelo, and K. Heidel, “A Process for Capturing CO2 from the Atmosphere,” Joule, vol. 2, no. 8, pp. 1573–1594, Aug. 2018, doi: 10.1016/j.joule.2018.05.006.
5. K. An, A. Farooqui, and S. T. McCoy, “The impact of climate on solvent-based direct air capture systems,” Appl Energy, vol. 325, Nov. 2022, doi: 10.1016/j.apenergy.2022.119895.
6. Q. Shu, L. Legrand, P. Kuntke, M. Tedesco, and H. V. M. Hamelers, “Electrochemical Regeneration of Spent Alkaline Absorbent from Direct Air Capture,” Environ Sci Technol, vol. 54, no. 14, pp. 8990–8998, Jul. 2020, doi: 10.1021/acs.est.0c01977.
7. E. O. Arwa and K. R. Schell, “Batteries or silos: Optimizing storage capacity in direct air capture plants to maximize renewable energy use,” Appl Energy, vol. 355, p. 122345, Feb. 2024, doi: 10.1016/j.apenergy.2023.122345.
8. H. Nami, F. Mohammadkhani, and F. Ranjbar, “Utilization of waste heat from GTMHR for hydrogen generation via combination of organic Rankine cycles and PEM electrolysis,” Energy Convers Manag, vol. 127, pp. 589–598, Nov. 2016, doi: 10.1016/j.enconman.2016.09.043.
9. D. J. Singh Aulakh, K. G. Boulama, and J. G. Pharoah, “On the reduction of electric energy consumption in electrolysis: A thermodynamic study,” Int J Hydrogen Energy, vol. 46, no. 33, pp. 17084–17096, May 2021, doi: 10.1016/j.ijhydene.2021.02.161.
10. Z. Wang, X. Wang, Z. Chen, Z. Liao, C. Xu, and X. Du, “Energy and exergy analysis of a proton exchange membrane water electrolysis system without additional internal cooling,” Renew Energy, vol. 180, pp. 1333–1343, Dec. 2021, doi: 10.1016/j.renene.2021.09.037.
11. C. Yilmaz and M. Kanoglu, “Thermodynamic evaluation of geothermal energy powered hydrogen production by PEM water electrolysis,” Energy, vol. 69, pp. 592–602, May 2014, doi: 10.1016/j.energy.2014.03.054.
12. S. Sharifian, N. Asasian Kolur, and M. Harasek, “Transient simulation and modeling of photovoltaic-PEM water electrolysis,” Energy Sources, Part A: Recovery, Utilization and Environmental Effects, vol. 42, no. 9, pp. 1097–1107, May 2020, doi: 10.1080/15567036.2019.1602220.
13. W. Li, H. Tian, L. Ma, Y. Wang, X. Liu, and X. Gao, “Low-temperature water electrolysis: fundamentals, progress, and new strategies,” Materials Advances, vol. 3, no. 14. Royal Society of Chemistry, pp. 5598–5644, May 17, 2022. doi: 10.1039/d2ma00185c.

© 2024 by the authors. Licensed to PSEcommunity.org and PSE Press. This is an open access article under the creative commons CC-BY-SA licensing terms. Credit must be given to creator and adaptations must be shared under the same terms. See https://creativecommons.org/licenses/by-sa/4.0/